A mathematical model and quantitative comparison of the small RNA circuit in the *Vibrio harveyi* and *Vibrio cholerae* quorum sensing systems

2013 Phys. Biol. 10 046007

(http://iopscience.iop.org/1478-3975/10/4/046007)

Phys. Biol. **10** (2013) 046007 (15pp) doi:10.1088/1478-3975/10/4/046007

A mathematical model and quantitative comparison of the small RNA circuit in the *Vibrio harveyi* and *Vibrio cholerae* quorum sensing systems

G A M Hunter, F Guevara Vasquez and J P Keener

Mathematics Department, University of Utah, 155 E 1400 S, Salt Lake City, UT 84112, USA

E-mail: keener@math.utah.edu

Received 3 April 2013
Accepted for publication 11 June 2013
Published 3 July 2013
Online at stacks.iop.org/PhysBio/10/046007

Abstract

Quorum sensing is the process by which bacteria regulate their gene expression based on the local cell-population density. The quorum sensing systems of *Vibrio harveyi* and *Vibrio cholerae* are comprised of a phosphorelay cascade coupled to a small RNA (sRNA) circuit. The sRNA circuit contains multiple quorum regulated small RNA (Qrr) that regulate expression of the homologous master transcriptional regulators LuxR (in *V. harveyi*) and HapR (in *V. cholerae*). Their quorum sensing systems are topologically similar and homologous thereby making it difficult to understand why repression of HapR is more robust than LuxR to changes in Qrr. In this work we formulate and parameterize a novel mathematical model of the *V. harveyi* and *V. cholerae* sRNA circuit. We parameterize the model by fitting it to a variety of empirical data from both species. We show that we can distinguish all of the parameters and that the parameterizations (one for each species) are robust to errors in the data. We then use our model to propose some experiments to identify and explain kinetic differences between the species. We find that *V. cholerae* Qrr are more abundant and more sensitive to changes in LuxO than *V. harveyi* Qrr and argue that this is why expression of HapR is more robust than LuxR to changes in Qrr.

1. Introduction

Quorum sensing is a regulatory system by which a bacterium coordinates its gene expression with neighboring bacteria based on the local cell-population density. Genes regulated by quorum sensing systems include those responsible for the production of toxins, biofilm, type III secretion factors, and bioluminescence. Quorum sensing systems are thought to provide some fitness benefit to bacteria. For example, a bacterial colony coordinating production of toxins would have a better chance of overwhelming a host's immune response than if each bacterium worked independently [1]. A typical quorum sensing response is characterized by a sudden change in gene expression at some critical cell-population density, although gene regulation is also mediated by environmental factors such as the preferred carbon source [2] and other unidentified factors [3]. Quorum sensing systems are found in a variety of bacteria and, as such, are thought to be common to all bacteria [4–10]. Research into quorum sensing systems continues to expand our understanding of gene expression and has the potential to develop novel therapies to combat bacteria whose virulence factors are quorum regulated [9, 11, 12].

Vibrio harveyi and *Vibrio cholerae* are pathogenic marine bacteria that use similar quorum sensing systems to regulate their respective virulence factors (see figure 1). Each quorum sensing system is comprised of two distinct pathways: a phosphorelay cascade that integrates cell-population density information and a small RNA (sRNA) circuit that regulates expression of all quorum sensing target genes via a transcriptional regulatory protein called LuxR in *V. harveyi* and HapR in *V. cholerae* [9]. In *V. harveyi*, three distinct autoinducers (HAI-1, AI-2, and CAI-1) are synthesized at

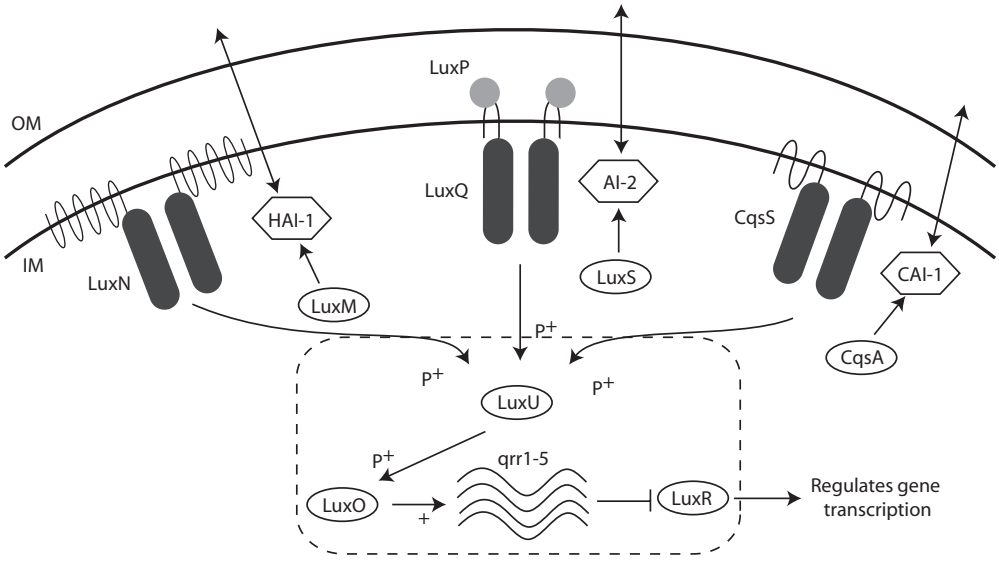

Figure 1. Overview of the *V. harveyi* quorum sensing circuit. Three phosphorelay cascades work in parallel to control the ratio of LuxO to LuxO-P based on local cell-population density. Five sRNA, *qrr1-5*, then regulate expression of quorum sensing target genes including the master transcriptional regulator LuxR, which upregulates downstream virulence factors. The *V. cholerae* quorum sensing circuit is nearly identical to that of *V. harveyi* except *V. cholerae* has only two phosphorelay cascades and four sRNA. All components in the *V. cholerae* quorum sensing system are homologous to those in *V. harveyi*. IM: inner membrane, OM: outer membrane.

some basal level by enzymes called autoinducer synthases (LuxM, LuxS, CqsA). For each autoinducer, there is a corresponding membrane bound receptor to which it binds: LuxN (binds HAI-1), LuxPQ (binds AI-2), and CqsS (binds CAI-1) [10, 7, 13, 14]. The autoinducers freely diffuse through the cell membrane [15] and disperse into the local environment leaving the receptors unbound at low cell-population density (LCD). When unbound, the receptors function as kinases and dephosphorylate high energy phosphate molecules. The phosphate is transferred to LuxU, a phosphorelay protein, that, again, transfers the phosphate to LuxO [7]. LuxO-P activates transcription of five distinct small RNA (sRNA) called quorum regulated RNA (*qrr1-5*). Qrr regulate the expression of *luxR* post transcriptionally by binding the *luxR* mRNA to prevent its translation [16–19]. Therefore, at LCD, Qrr is abundant and *luxR* is repressed.

Conversely, at high cell-population density (HCD) intercellular autoinducer concentration rises leading the autoinducer to bind their respective receptor [20, 5, 21]. When bound, the receptors undergo a conformational change that changes their function to a phosphatase [22, 23]. In this state, the flow of the phosphates is reversed as the receptors dephosphorylate LuxU. This results in a decrease in LuxO-P and in Qrr. Therefore, LuxR is derepressed and regulates downstream quorum sensing genes [7, 24–26].

The quorum sensing system of *V. cholerae* is nearly identical to that of *V. harveyi* with a few minor topological differences whose effects, we assume, are negligible. *V. cholerae* has four Qrr (*qrr1-4*) and two autoinducer receptors (LuxPQ and CqsS) rather than, respectively, the five and three found in *V. harveyi*. Experiments show that *qrr5* in *V. harveyi* is not quorum regulated [27, 17], so we ignore *qrr*5 for this work. The additional autoinducer receptor in *V. harveyi* means that *V. harveyi* responds to three, rather than two, autoinducers. However, information from the receptors is integrated into one signal—the ratio of LuxO-P to LuxO [28], so the number of different phosphorelay cascades cannot be distinguished for a given ratio of LuxO to LuxO-P alone. Therefore, we assume that these topological differences do not significantly alter the response of one species relative to the other.

In fact, the *V. harveyi* and *V. cholerae* quorum sensing systems are very similar. Sequence analysis of the genes and proteins in the *V. cholerae* circuit shows that the components in *V. cholerae* are homologous to those in *V. harveyi*. Furthermore, AI-2 and CAI-1 have the same chemical structure between both species. This means that *V. cholerae* responds to AI-2 and CAI-1 taken from *V. harveyi* and vice versa. Consequently, the nomenclature for the components in each circuit is identical with the exception of HapR in *V. cholerae*—the *V. harveyi* LuxR homologue [15, 7]. These topological and genetic similarities make it difficult to determine if and why *V. harveyi* and *V. cholerae* respond differently to identical stimuli. In particular, experiments show that HapR repression in *V. cholerae* strains with just one Qrr is nearly identical to HapR repression in a wild-type strain [17], yet LuxR repression depends on the number and type of Qrr present in isogenetic *V. harveyi* strains [16].

In this work, we formulate and parameterize a novel mathematical model of the sRNA circuit to identify and explain the mechanisms underlying the kinetic differences between *V. harveyi* and *V. cholerae*. First we use data from at least four experiments for each species to find 35 and 33 physiologically relevant parameters representing *V. harveyi* and *V. cholerae*, respectively, by solving a constrained, nonlinear least-squares problem. We solve the problem using Matlab's nonlinear least-squares solver 'lsqnonlin' aided by the exact Jacobian of the model of each experiment and show that our model is representative of the *V. harveyi* and *V. cholerae* sRNA circuits.

We then propose a series of simple experiments that would help to identify novel kinetic differences between the species. We find that Qrr are more abundant in *V. cholerae* than in *V. harveyi* and that *V. harveyi* and *V. cholerae* Qrr are sensitive to changes in LuxR and LuxO, respectively. As a corollary of these results, we argue and demonstrate that this explains why dosage compensation is stronger in *V. cholerae* than in *V. harveyi*. Our results refine the hypothesis of Svenningsen *et al* who suggested that the differences in LuxR/HapR repression were a consequence of stronger dosage compensation in *V. cholerae* than in *V. harveyi*. [29]. Lastly, we argue that saturation of Hfq, a protein chaperon that stabilizes Qrr, by Qrr is essential for the robust repression of target mRNA.

2. Materials and methods

In what follows, we derive a set of differential equations that model the reaction kinetics of the sRNA circuit. Although the focus of this work is on the sRNA circuit in *V. harveyi* and *V. cholerae*, we need a simple model of the *V. harveyi* phosphorelay cascade to incorporate more experimental data into the parameterization of our model of the *V. harveyi* sRNA circuit. To this end, Swem *et al* parameterized a model of the *V. harveyi* autoinducer receptors and found that the difference in free energy between the kinase and phosphatase states is

$$\frac{\Delta G}{k_B T} = -2.3 + \ln\left(\frac{1+\mathrm{AI}}{1+10^{-6}\mathrm{AI}}\right), \tag{1}$$

where AI is the concentration (nM) of autoinducer [30]. Assuming there is only one phosphorelay cascade, the input for the sRNA circuit is the ratio of LuxO-P, O_P, to LuxO, O [28]. At steady-state, $O_P = \Gamma O$, where the equilibrium constant, Γ, is of the form $\Gamma = \exp\left(-\frac{\Delta G}{k_B T}\right)$. Therefore, our simple model of the phosphorelay cascade is:

$$\Gamma = \exp\left(2.3 - \ln\left(\frac{1+\mathrm{AI}}{1+10^{-6}\mathrm{AI}}\right)\right). \tag{2}$$

If the autoinducer concentration is known, then we use (2) to relate the concentration of autoinducer to Γ, otherwise we treat Γ as a parameter representative of the cell-population density. Note that LCD corresponds to large Γ, while HCD corresponds to small Γ.

2.1. Overview of the sRNA circuit

The sRNA circuit is central to the *V. harveyi* and *V. cholerae* quorum sensing system (see figure 2). Small RNA are short fragments of non-coding RNA that regulate gene expression post-transcriptionally [18]. Qrr repress mRNA expression by binding the ribosomal binding site of target mRNA that, thereby, prevents its translation [16, 19]. The *V. harveyi* and *V. cholerae* Qrr are highly conserved within and between each species including an identical 32bp sequence responsible for its association with mRNA [16]. At the start of the sRNA circuit, *qrr* expression is regulated by the ratio of LuxO-P to LuxO [28]. LuxO-P binds the *qrr* promoter to activate its expression. Each Qrr is rapidly degraded unless they bind Hfq [31], a protein chaperon, which also aids *qrr* to bind target

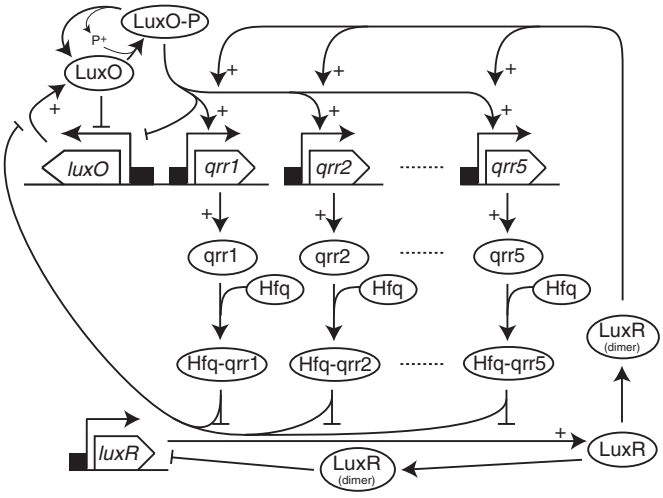

Figure 2. Overview of the *V. harveyi* sRNA circuit. LuxO-P activates *qrr* expression, which bind to target mRNA via Hfq to prevent translation of the mRNA into an active protein. Four different regulatory mechanisms aid to control precisely the expression of target mRNA. LuxR (as a dimer) and LuxO are autoregulatory as each binds their own promoter to limit transcription. LuxR (as a dimer) enhances *qrr* expression by binding the *qrr* promoter via the LuxR-Qrr feedback. Lastly, *qrr* target and prevent translation of *luxO* mRNA via the LuxO-Qrr feedback. The *V. cholerae* sRNA circuit is topologically identical and homologous to *V. harveyi* except that *V. cholerae* has four, rather than five, sRNA and HapR is the LuxR homologue.

mRNA. The pairing of *qrr* with mRNA results in their mutual degradation and leaves Hfq unchanged [16].

There are four regulatory pathways in the sRNA circuit to maintain precise control of *luxR/hapR* expression [7]. The first two pathways are autoregulatory loops. LuxR/HapR regulates its own expression by forming as a dimer and binding its own promoter to limit its transcription [32, 33]. Similarly, LuxO and *qrr1* are divergently transcribed, so LuxO-P limits *luxO* transcription when it binds the *qrr1* promoter. Although only LuxO-P activates *qrr1* transcription, experiments show that both LuxO-P and LuxO equally inhibit *luxO* expression [19].

The remaining two pathways involve feedback between Qrr and the target mRNA and, as such, are called the LuxR/HapR-Qrr and LuxO-Qrr feedback. LuxR/HapR enhances the expression of *qrr* when LuxO-P is present [34, 27]. This is done by LuxR binding directly to the *qrr* promoter, while HapR does so indirectly via a currently unknown intermediary. Lastly, Qrr regulate LuxO expression in the same manner as Qrr regulates LuxR/HapR expression and is called the LuxO-Qrr feedback [29, 19]. These autoregulatory and feedback regulatory pathways control the onset and transition to/from LCD and HCD [29, 19].

2.2. Model of the sRNA circuit

In this section we derive our model of the sRNA circuit. We begin with the reactions governing the expression of *luxO*, *o*, and *luxR/hapR*, *r*, in the absence of *qrr*. These reactions are summarized in figure 3.

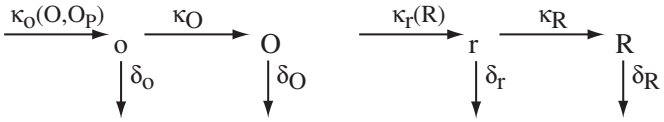

Figure 3. Reactions governing the expression of *luxO* and *luxR* in the absence of *qrr*.

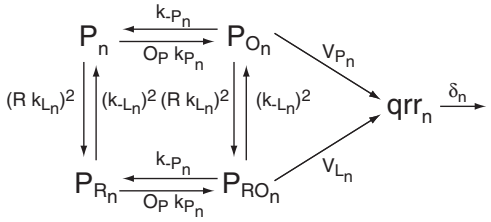

Figure 4. Qrr promoter model. We define four states representing the probability that the promoter is bound by LuxR and/or LuxO-P.

We assume that there is a basal rate of expression of *luxO* that is inhibited equally by both LuxO and LuxO-P [19]. Therefore, the transcription rate of *luxO* is

$$\kappa_o(O, O_P) = \frac{V_o}{1 + K_O(O + O_P)}. \tag{3}$$

The *luxO* mRNA is transcribed at a rate proportional to its concentration and degraded at a rate proportional to its concentration and similarly for LuxO. The reactions governing the expression of *luxR* are identical in form to those governing expression of *luxO*. The main difference is that the *luxR* transcription rate is partially inhibited by a LuxR dimer [33, 32], so we take

$$\kappa_r(R) = V_{r0} + \frac{V_r}{1 + (K_r R)^2}. \tag{4}$$

The reactions governing the expression of the nth species of *qrr* are summarized in figure 4. LuxO-P activates *qrr* expression and a LuxR/HapR dimer enhances this expression. To model this process, we introduce four different states for the *qrr* promoter that represent the probability that the promoter is unbound, P_n, bound by a LuxR/HapR dimer, P_{R_n}, bound by LuxO-P, P_{O_n}, or bound by LuxO-P and a LuxR/HapR dimer, P_{RO_n} [7]. We also assume that the rates of *qrr* transcription for the latter two states are different.

The corresponding equations governing the states of the *qrr* promoter are:

$$1 = P_{R_n} + P_{O_n} + P_{OR_n} + P_n, \tag{5}$$

$$\frac{dP_{R_n}}{dt} = (k_{L_n}R)^2 P_n + k_{-P_n} P_{RO_n} - (k_{-L_n}^2 + O_P k_{P_n}) P_{R_n}, \tag{6}$$

$$\frac{dP_{O_n}}{dt} = k_{P_n} O_P P_n + (k_{-L_n})^2 P_{RO_n} - ((Rk_{L_n})^2 + k_{-P_n}) P_{O_n}, \tag{7}$$

$$\frac{dP_{RO_n}}{dt} = k_{P_n} O_P P_{R_n} + (Rk_{L_n})^2 P_{O_n} - ((k_{-L_n})^2 + k_{-P_n}) P_{O_n}, \tag{8}$$

$$\frac{dq_n}{dt} = V_{P_n} P_O + V_{L_n} P_{RO_n} - \delta_n q_n. \tag{9}$$

We solve for the steady-state probabilities P_{RO_n} and P_{O_n} and rewrite (9) as:

$$\frac{dq_n}{dt} = \frac{K_{P_n} O_P}{1 + K_{P_n} O_P} \frac{V_{P_n} + V_{L_n}(K_{L_n}R)^2}{1 + (K_{L_n}R)^2} - \delta_n q_n. \tag{10}$$

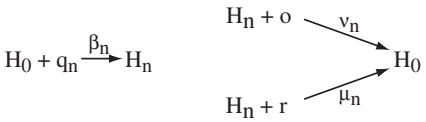

Figure 5. Reactions for the degradation of mRNA by *qrr*. Each *qrr* binds Hfq that then targets *luxR* and *luxO* mRNA. Once bound, the sRNA–mRNA dimers unbind from Hfq and are degraded while Hfq remains intact. The net result of this reaction is the loss of one *qrr* for each mRNA.

The final part of the sRNA model describes the repression of target mRNA by Qrr and is summarized in figure 5. Given that Hfq is pleiotropic and abundant in cells [35, 36], we assume that the total concentration of Hfq available for quorum sensing is constant, H_0. Hfq aids in repressing target mRNA by stabilizing *qrr* and facilitating *qrr* to bind target mRNA. Once *qrr* binds its target mRNA, the sRNA–mRNA dimer unbinds Hfq leaving it intact, and the sRNA–mRNA dimer is eventually degraded [16]. The net result of this reaction is the loss of one sRNA and mRNA.

In summary, the complete set of equations governing the sRNA circuit is,

$$\Gamma = \exp\left(2.3 - \ln\left(\frac{1 + \mathrm{AI}}{1 + 10^{-6}\mathrm{AI}}\right)\right), \tag{11}$$

$$\frac{dR}{dt} = \kappa_R r - \delta_R R, \tag{12}$$

$$\frac{dO}{dt} = \kappa_O o - \delta_O O, \tag{13}$$

$$\frac{dr}{dt} = V_{r0} + \frac{V_r}{1 + (K_R R)^2} - \sum_{i=1}^{4} \mu_i H_i r - \delta_r r, \tag{14}$$

$$\frac{do}{dt} = \frac{V_o}{1 + K_O(1 + \Gamma)O} - \sum_{i=1}^{4} \nu_i H_i o - \delta_o o, \tag{15}$$

$$\frac{dq_n}{dt} = \frac{K_{P_n}\Gamma O}{1 + K_{P_n}\Gamma O} \frac{V_{P_n} + V_{L_n}(K_{L_n}R)^2}{1 + (K_{L_n}R)^2} - \beta_n \left(H_0 - \sum_{i=1}^{4} H_i\right) q_n - \delta_n q_n, \tag{16}$$

$$\frac{dH_n}{dt} = \beta_n \left(H_0 - \sum_{i=1}^{4} H_i\right) q_n - \mu_n H_n r - \nu_n H_n o, \tag{17}$$

where $n = 1, \ldots, 4$ corresponds to the index of nth species of sRNA. We assume that there are only four rather than five Qrr since *qrr5* is not quorum regulated in *V. harveyi*.

We now non-dimensionalize the equations to simplify their parameterization. We first define the characteristic concentrations:

$$r_M = \frac{V_{r0} + V_r}{\delta_r}, \quad o_0 = \frac{V_o}{\delta_o}, \quad O_0 = \frac{\kappa_O}{\delta_O} o_0,$$
$$R_0 = \frac{\kappa_R}{\delta_R} r_M, \quad Q_n = \frac{V_{P_n}}{\delta_n}. \tag{18}$$

We then rescale the variables in our model using the characteristic concentrations as follows:

$$r = r_M\widehat{r}, \qquad R = R_0\widehat{R}, \qquad H_n = H_0\widehat{H}_n,$$
$$o = o_0\widehat{o}, \qquad O = O_0\widehat{O}, \qquad q_n = Q_n\widehat{q}_n. \tag{19}$$

Next, we define the following dimensionless parameters:

$$E_{q_n} = \frac{H_0\beta_n}{\delta_n}, \quad E_{r_n} = \frac{H_0\mu_n}{\delta_r}, \quad E_{o_n} = \frac{H_0\nu_n}{\delta_o}$$
$$V_{q_n} = \frac{V_{L_n}}{V_{P_n}}, \quad V_{r_n} = \frac{V_{r0}+V_r}{V_{P_n}}, \quad V_{or} = \frac{V_o}{V_{r0}+V_r},$$
$$\widehat{K}_{P_n} = K_{P_n}O_0, \quad \widehat{K}_{L_n} = K_{L_n}R_0, \quad \widehat{K}_O = K_OO_0,$$
$$\widehat{K}_R = K_RR_0, \quad r_0 = \frac{V_{r0}}{V_{r0}+V_r}. \tag{20}$$

At steady-state, the model simplifies to:

$$\Gamma = \exp\left(2.3 - \ln\left(\frac{1+\mathrm{AI}}{1+10^{-6}\mathrm{AI}}\right)\right), \tag{21}$$

$$0 = r_0 + \frac{1-r_0}{1+(\widehat{K}_Rr)^2} - \left(\sum_{n=1}^{4} E_{r_n}H_n + 1\right) r, \tag{22}$$

$$0 = \frac{1}{1+\widehat{K}_O(1+\Gamma)o} - \left(\sum_{n=1}^{4} E_{o_n}H_n + 1\right) o, \tag{23}$$

$$0 = \frac{\widehat{K}_{P_n}\Gamma o}{1+\widehat{K}_{P_n}\Gamma o}\frac{1+V_{q_n}(\widehat{K}_{L_n}r)^2}{1+(\widehat{K}_{L_n}r)^2} - \left(E_{q_n}\left(1-\sum_{m=1}^{4}H_m\right)+1\right) q_n, \tag{24}$$

$$0 = E_{q_n}\left(1-\sum_{m=1}^{4}H_m\right) q_n - V_{r_n}(E_{r_n}r + V_{or}E_{o_n}o)H_n. \tag{25}$$

$\widehat{K}_R$ and $\widehat{K}_O$ represent the LuxR/HapR and LuxO autoregulation, respectively. V_{q_n} and $\widehat{K}_{L_n}$ represent the LuxR/HapR-Qrr feedback, and E_{o_n} and V_{or} represent the LuxO-Qrr feedback. For simplicity, we drop the '$\widehat{\ }$' notation on o, r, q_n, and H_n.

3. Results and discussion

In this section we describe how the empirical data from *V. harveyi* and *V. cholerae* were used to parameterize our model. Furthermore, we show that our model with a parameterization for each species agrees well with the data and that the model is representative of quorum sensing in *V. harveyi* and *V. cholerae*. Lastly, we use our model to predict novel behavior in *V. harveyi* and *V. cholerae*. To parameterize our model, we formulated and solved the following constrained, nonlinear least-squares problem:

$$\min_{\boldsymbol{p}\geqslant\boldsymbol{a}} ||\boldsymbol{F}(\boldsymbol{p}) - \boldsymbol{d}||^2. \tag{26}$$

Here $\boldsymbol{d}$ is a vector containing the raw data from each experiment and $\boldsymbol{p}$ is a vector representing the wild-type parameterization. The constraint $\boldsymbol{p} \geqslant \boldsymbol{a}$ is necessary to ensure that $V_{r_n} \geqslant 1$ for all n (i.e. so that LuxR/HapR only enhances Qrr expression) and that all of the remaining parameters are non-negative. We define $F_i(\boldsymbol{p})$ as a model of the experiment corresponding to the ith data point. We then store all the models together in the vector $\boldsymbol{F}(\boldsymbol{p})$. Therefore, $F_i(\boldsymbol{p}) - d_i$ is the error associated with modeling the i'th experiment, while $||\boldsymbol{F}(\boldsymbol{p})-\boldsymbol{d}||^2$ represents the total error between our model and all of the experiments for the given wild-type parameterization. A detailed discussion of the data and how we modeled each experiment are provided in the sections that follow. We solved the problem using Matlab's 'lsqnonlin' function. To improve the accuracy and rate of convergence, we calculated the Jacobian of $\boldsymbol{F}(\boldsymbol{p})$ exactly by differentiating (22)–(25) and using these derivatives to compute $\nabla F_i(\boldsymbol{p})$.

In an attempt to find the global minimum, we solved the problem using several different initial guesses that spanned a feasible set containing the solution. Each initial guess is a vector of uniformly distributed random numbers generated over the feasible set of wild-type parameters. To find a reasonable feasible set for all of the parameters, we started with a large feasible set and manually refined it so that the solutions from randomly generated parameter vectors remained inside the new feasible set. We terminated the nonlinear least-squares solver either when the residual was below a certain threshold (i.e. $||\boldsymbol{F}(\boldsymbol{p}) - \boldsymbol{d}||^2 \leqslant 10^{-4}$) or after some finite number of iterations. The parameterization for each species and corresponding final feasible set is summarized in table 1.

In the next two sections we describe the experiments and how we modeled them in each function $F_i(\boldsymbol{p})$. Although the details of $F_i(\boldsymbol{p})$ are different, they all have the following general structure. We created a parameterization for each mutant strain in the experiment by modifying the wild-type parameterization. For example, to model a strain without the LuxO-Qrr feedback, we set $E_{o_n} = V_{or} = 0$ in the wild-type parameterization. Next, we computed the steady-state solution of each strain by solving (22)–(25) and using the exact Jacobian of the nonlinear system of equations. Lastly, we measured the steady-state quantities in our model that corresponded to those measured in the experiments such as the ratio of the steady-state concentration of *luxR*/*hapR* in a wild-type strain relative to a mutant strain.

3.1. V. harveyi parameterization

In this section we describe the *V. harveyi* data we used to fit the model to. The first two experiments below are used to parameterize r_0, K_R, and K_{L_n} ($n = 1, 2, 3, 4$) because those data are uniquely determined by those parameters. K_R and K_{L_n} are related to their dimensionless counterparts by the characteristic concentration of LuxR, R_0. We simultaneously fit the rest of the parameters to the remaining data using the formulation described by (26) treating R_0 as an unknown parameter rather than $\widehat{K}_{L_n}$ and $\widehat{K}_R$. The full *V. harveyi* parameterization is shown in table 1.

3.1.1. LuxR autoregulation. Chatterjee *et al* identified the regions of the *luxR* promoter involved in the autoregulation of LuxR and used mobility-shift assays to measure the proportion of *luxR* promoters bound at a given concentration of LuxR

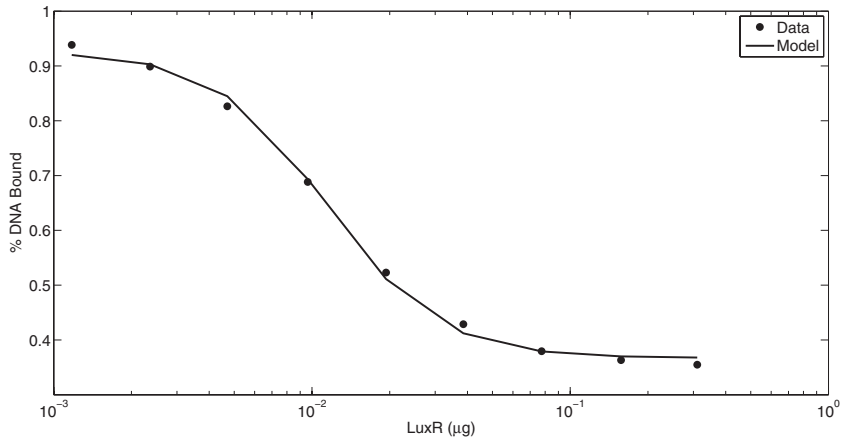

Figure 6. A comparison between the data (dotted points) and our parameterization results (solid curve) of the proportion of LuxR promoters bound by LuxR as the concentration of LuxR varies. The data was generated using mobility-shift assays and taken from figure 6A of [32] and shows that LuxR binds its own promoter. We used this data to parameterize our model of the LuxR promoter, $r_0 + (1 - r_0)/(1 + (K_R R)^2)$, and found that $K_R = 0.0250\ \ (\mu g)^{-1}$ and $r_0 = 0.38$.

Table 1. Parameters and their corresponding feasible set for *V. harveyi* and *V. cholerae*. All parameters are dimensionless except for R_0 as indicated.

	V. harveyi		*V. cholerae*	
Parameter	Value	Feasible set	Value	Feasible set
r_0	3.67×10^{-1}	–	2.96×10^{-1}	[0, 0.6]
$\widehat{K}_R$	1.38×10^{1}	–	9.03×10^{-1}	[0, 1]
$\widehat{K}_O$	1.80	[1, 7]	1.55×10^{1}	[5, 35]
Γ_{LCD}	1.82×10^{-2}	[0, 1]	2.15×10^{-1}	[0.15, 0.35]
Γ_{HCD}	1.94×10^{-1}	[0, 0.07]	–	–
$\widehat{K}_{P_1}$	3.62×10^{-1}	[0, 3]	2.65	[2, 3]
$\widehat{K}_{P_2}$	3.60	[1, 11]	3.94×10^{1}	[26, 42]
$\widehat{K}_{P_3}$	7.30	[2, 20]	9.36×10^{-1}	[0.7, 1]
$\widehat{K}_{P_4}$	1.13	[0, 7]	8.89	[7, 10]
$\widehat{K}_{L_1}$	0	–	1.84×10^{2}	[120, 260]
$\widehat{K}_{L_2}$	2.21×10^{1}	–	3.04×10^{1}	[25, 55]
$\widehat{K}_{L_3}$	1.38×10^{1}	–	1.08×10^{1}	[8.5, 12]
$\widehat{K}_{L_4}$	2.95×10^{1}	–	4.77×10^{1}	[33, 50]
E_{r_1}	5.05×10^{5}	$[1 \times 10^{5}, 9 \times 10^{5}]$	8.36×10^{1}	[35, 95]
E_{r_2}	1.83×10^{3}	[250, 2000]	2.87×10^{2}	[55, 320]
E_{r_3}	2.31×10^{1}	[3, 70]	2.98×10^{2}	[150, 500]
E_{r_4}	1.08×10^{3}	$[250, 2.2 \times 10^{3}]$	4.76×10^{1}	[40, 700]
E_{o_1}	1.35×10^{-2}	[0, 5]	1.07×10^{1}	[2.5, 12]
E_{o_2}	1.20×10^{1}	[0, 25]	6.99×10^{1}	[14, 80]
E_{o_3}	2.33×10^{2}	[75, 300]	1.21×10^{2}	[100, 400]
E_{o_4}	8.18×10^{-1}	[0, 4]	2.95×10^{-1}	[0, 0.3]
E_{q_1}	4.65×10^{-3}	[0, 0.2]	2.98×10^{-1}	[0, 3]
E_{q_2}	3.31	[0, 35]	2.31×10^{-3}	[0, 0.8]
E_{q_3}	9.57	[5, 40]	1.58×10^{2}	[0, 180]
E_{q_4}	1.74×10^{-1}	[0, 1.25]	4.33×10^{1}	[0, 75]
V_{q_1}	0	–	4.99	[4, 6]
V_{q_2}	1.90	[1.5, 2.2]	1.91	[1.25, 2.5]
V_{q_3}	2.28	[2.1, 2.5]	1.41×10^{1}	[12, 16]
V_{q_4}	2.56	[2.4, 2.8]	3.65	[3, 4.5]
V_{r_1}	1.44	[1, 5]	7.81×10^{-2}	[0, 0.45]
V_{r_2}	5.80	[0, 7]	8.49×10^{-4}	[0.15, 0.45]
V_{r_3}	5.83×10^{-1}	[0 2]	2.51×10^{-2}	[0, 0.05]
V_{r_4}	4.63	[2, 5]	5.57×10^{-1}	[0.2, 0.8]
V_{or}	$1.28 \cdot 10^{1}$	[2, 22]	2.42	[1, 5]
R_0 (nM)	5.16×10^{2}	[200, 600]	–	–

[32]. We used this data to parameterize our model of the *luxR* promoter model, $r_0 + (1 - r_0)/(1 + (K_R R)^2)$. The data (dots) and the results from our parameterization (solid curve) are shown in figure 6. We found that $K_R \approx 0.0250\ \ (\mu g)^{-1}$ and that $r_0 \approx 0.38$.

3.1.2. LuxR affinity to the qrr promoters. Tu *et al* used mobility-shift assays to show that LuxR enhances *qrr* expression by binding directly to each *qrr* promoter [27]. We set $K_{L_1} = 0\ \text{nM}^{-1}$, $K_{L_2} = (25\ \text{nM})^{-1}$, $K_{L_3} = (40\ \text{nM})^{-1}$, and $K_{L_4} = (19\ \text{nM})^{-1}$ based on visual inspection of the data in figure 2 of their work [27].

3.1.3. LuxR-Qrr feedback at low and high cell density. Tu *et al* showed that LuxR enhances Qrr expression in *V. harveyi* when it binds the *qrr* promoter [27]. They created a Δ*luxR* and a *qrr*2, 3, $4^{luxR-bs}$ strain, which has a scrambled LuxR binding site in each *qrr* promoter to limit/prevent LuxR binding. Using quantitative real-time PCR analysis, they measured the level of *qrr* at low and at high cell density in a wild-type strain and each mutant strain. They present their results by normalizing the concentration of *qrr* by their corresponding wild-type concentration at LCD. The data, shown in figure 7 (left), shows that LuxR enhances *qrr2-4* expression and that there is little difference in *qrr* concentration between the mutant strains.

To model this experiment, we modified the wild-type parameterization to model the two mutant strains in the experiment: Δ*luxR* ($E_{r_n} = \widehat{K}_{L_n} = V_{q_n} = 0$), and *qrr*2, 3, $4^{luxR-bs}$ ($\widehat{K}_{L_n} = V_{q_n} = 0$). We also parameterize two different values of Γ that correspond to the different ratios of LuxO:LuxO-P at low and at high cell density (i.e. $\Gamma_{\text{LCD}} > \Gamma_{\text{HCD}}$). For each strain, we computed the steady-state concentration of each *qrr* at Γ_{LCD} and at Γ_{HCD}. Lastly, we normalized each *qrr* concentration by its corresponding concentration in the wild-type strain at LCD. Our final results (middle) and corresponding error (right) are shown in figure 7. The model agrees well with the data at both low and high cell density, although there is less agreement at HCD.

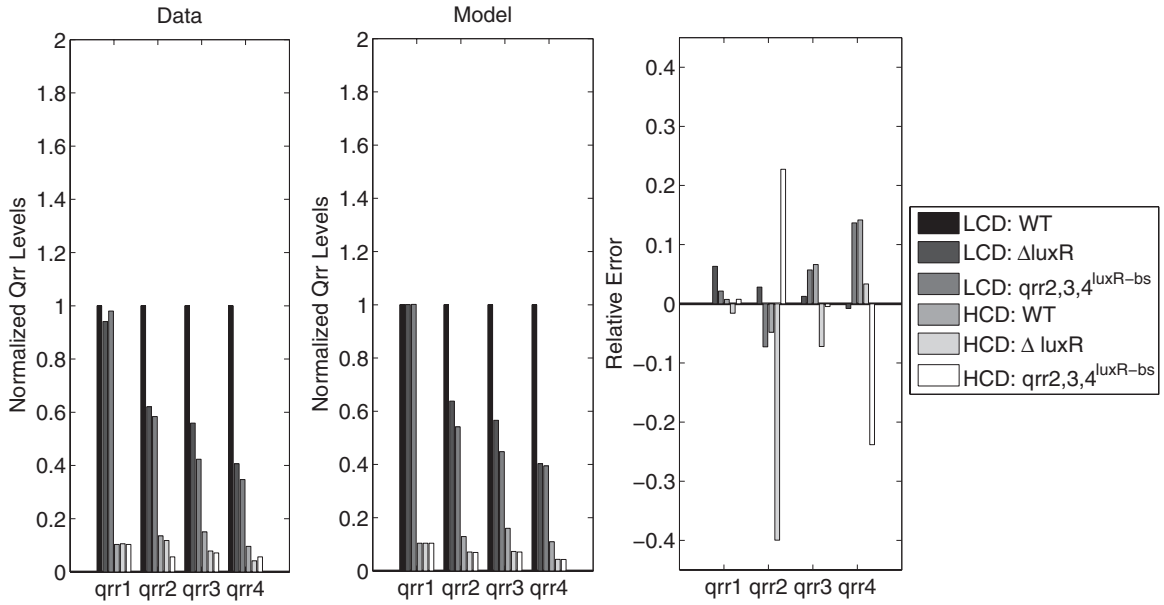

Figure 7. Comparison between the data [27] (left) and our results (center) of the fold change in the concentration of each Qrr in the absence of the LuxR-Qrr feedback at LCD and HCD. Three strains were used in the experiments: wild-type, $\Delta luxR$, and $qrr2, 3, 4^{luxR-bs}$ (one with a scrambled LuxR binding site in each Qrr promoter). The concentration of Qrr was measured in each strain at LCD and HCD and normalized by the concentration in the wild-type strain at LCD. The relative error of the results is shown on the right.

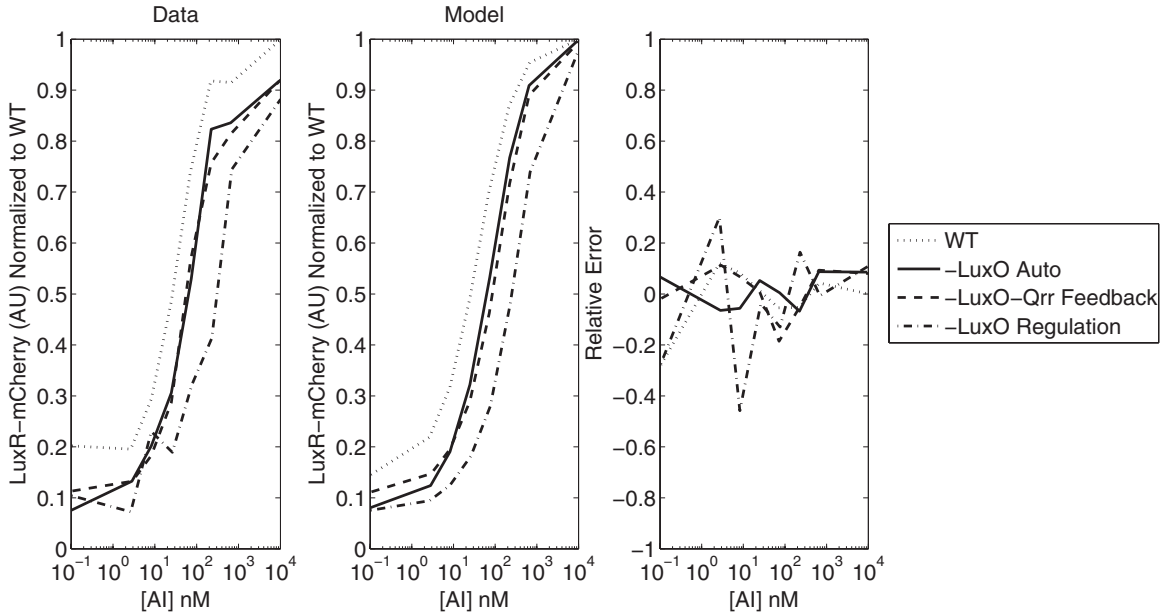

Figure 8. A comparison between the data [19] (left) and our results (middle) showing the florescence of the LuxR-mCherry construct over increasing autoinducer concentrations in wild-type, −LuxO-Auto, −LuxO-Qrr feedback, and −LuxO regulation strains. We normalized the data and our results to the LuxR-mCherry florescence in the wild-type strain at an autoinducer concentration of 10^4 nM. The error associated with our results (right) is largest when autoinducer concentrations are small, which also corresponds to when there is more uncertainty in the data.

3.1.4. Role of LuxO regulation in V. harveyi. Tu *et al* showed that LuxO regulation affects the onset of the LCD to HCD transition and the dynamic range of expression of quorum sensing target gene expression [19]. They introduced a LuxR-mCherry protein fusion into the *V. harveyi* chromosome at the native *luxR* locus in four different strains: wild-type, −LuxO-Auto, −LuxO-Qrr feedback, −LuxO regulation. The latter three strains lack LuxO autoregulation, LuxO-Qrr feedback, or both, respectively. They used single cell fluorescence microscopy to measure LuxR-mCherry in individual cells over a range of autoinducer concentrations for each strain as a means to infer *luxR* expression. Their results, in figure 8 (left), show that the onset of the LCD to HCD transition is shifted to larger autoinducer concentrations when LuxO regulation is

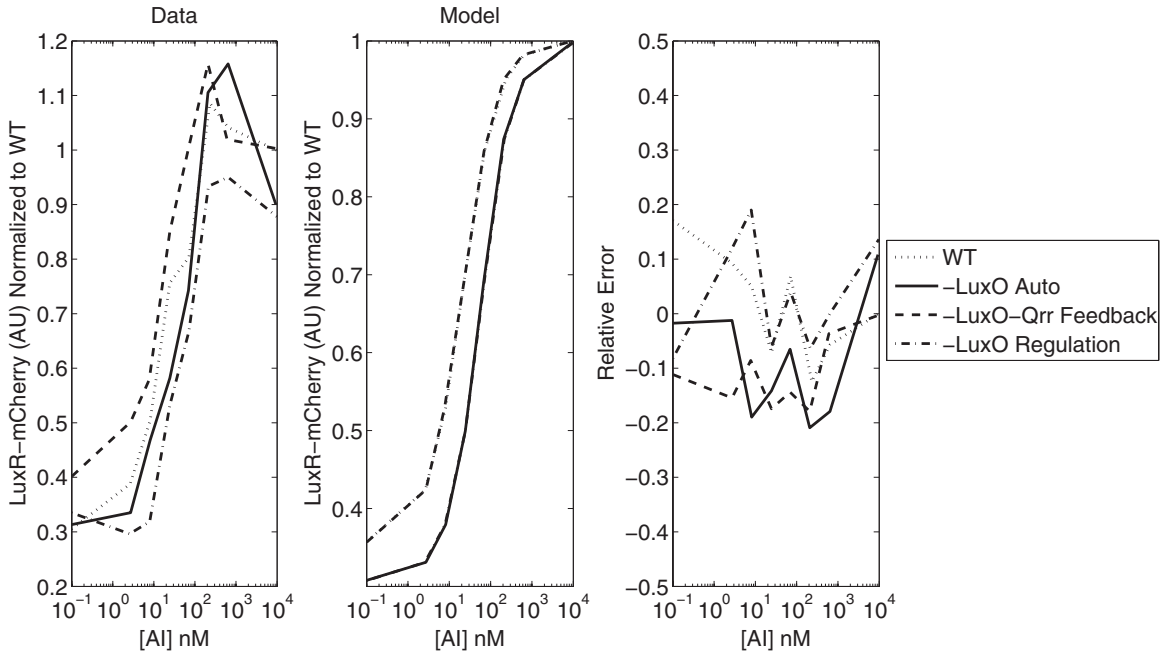

Figure 9. A comparison between the data [19] (left) and our results (middle) showing the florescence of the LuxR-mCherry construct over different autoinducer concentrations in wild-type, −LuxO-Auto, −LuxO-Qrr feedback, and −LuxO regulation strains containing *qrr*4 only. We normalized the data and our results to the LuxR-mCherry florescence in the wild-type strain at an autoinducer concentration of 10^4 nM. The error (right) shows that the repression of LuxR at low autoinducer concentrations in our model is much larger than that observed in the data.

removed. The data also show that there is little difference in LuxR expression between the −LuxO-Auto and −LuxO-Qrr feedback strains.

To model this experiment, we created parameterizations of each strain. Taking the parameterization of the wild-type strain, we set $\widehat{K}_O = 0$ for the −LuxO-Auto strain, $E_{o_n} = V_{or} = 0$ for the −LuxO-Qrr feedback strain, and $\widehat{K}_O = E_{o_n} = V_{or} = 0$ for the −LuxO regulation strain. Since fluorescence is expressed as a function of autoinducer concentration, we used (2) to relate Γ to the concentration of autoinducer in the data. We then computed the steady-state concentration of LuxR in each strain at every autoinducer concentration. Our results (middle) and corresponding error (right) are shown in figure 8. Our results reproduce the shift in the LuxR dose response curve for the various mutant strains. We note that the error is largest at LCD where there is more uncertainty in the data as well.

Tu *et al* repeated the experiment using strains with *qrr4* only. Their results in figure 9 (left) show a shift in the onset of the LCD to HCD transition similar to their previous results. Additionally, there is a three rather than a fivefold change in fluorescence from LCD to HCD. To model this experiment, we repeated the previous experiment taking $\widehat{K}_{P_1} = \widehat{K}_{P_2} = \widehat{K}_{P_3} = 0$ in all of the strains. Our results, figure 9 (middle), reflect a similar shift in the onset as the data, however, our results also show more repression of LuxR at LCD than what is reflected in the data.

3.2. *V. cholerae* parameterization

We parameterized the model to all of the *V. cholerae* data simultaneously by solving the problem described by (26). The *V. cholerae* experiments were all performed at the same optical density corresponding to LCD so there is only one value of Γ in our *V. cholerae* parameterization. In what follows, we describe the four *V. cholerae* experiments, how we modeled them, and discuss our results. The complete *V. cholerae* parameterization is shown in table 1.

3.2.1. HapR repression. Svenningsen *et al* showed that one *qrr* is sufficient to repress *hapR* to near wild-type levels [29]. They created four mutant strains that had only one type of *qrr* and a mutant strain without any *qrr*. Using real-time PCR analysis, they measured *hapR* concentration in each strain and normalized the *hapR* concentration by its concentration in the wild-type strain. Their results, figure 10 (left), show that all Qrr significantly repress *hapR* similar to wild-type levels especially *qrr*4.

To model this experiment, we used the wild-type parameterization and set $\widehat{K}_{P_n} = 0$ for each of the *n qrr* knocked out in the mutant strains, i.e. for the $+qrr2$ strain, we used the wild-type parameterization and set $\widehat{K}_{P_n} = 0$ for $n = 1, 3, 4$. To parameterize the Δqrr strain, we set $\widehat{K}_{P_n} = 0$ for all n. We then found the steady-state concentration of *hapR* in each strain then normalized each by the *hapR* concentration in the wild-type strain. A comparison between the data (left), model (center), and the relative error (right) is shown in figure 10. Our results show that the model agrees well with the data.

3.2.2. Dosage compensation. Svenningsen *et al* showed that *qrr* expression increases in the absence of one or more *qrr* in *V. cholerae*—a phenomenon they called dosage compensation

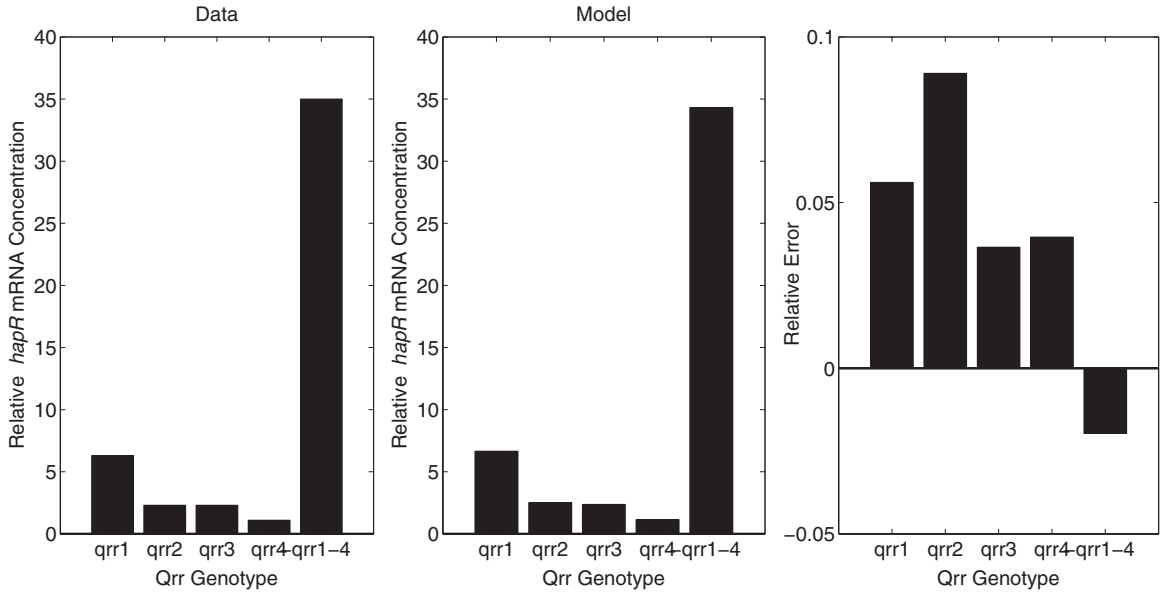

Figure 10. Comparison between the data [29] (left) and our results (middle) showing the fold change in LCD *hapR* mRNA concentration in a strain with at most one Qrr relative to *hapR* mRNA concentration a wild-type strain. The error (right) shows that the model is in good agreement with the data.

[29]. Using real-time PCR analysis, Svenningsen *et al* measured the concentrations of *hapR* and *qrr* in a wild-type, $\Delta qrr3$, $\Delta qrr2, 3$, and in a $\Delta qrr1, 2, 3$ strain at LCD. These data were then normalized to their corresponding wild-type levels. Their results show that, as each *qrr* is removed, the expression of the remaining *qrr* increases, while *hapR* remains relatively constant [29].

We model this experiment as follows. For the mutant strains, we modified the wild-type parameterization by setting $\widehat{K}_{P_n} = 0$ for the nth Qrr removed. We then computed the steady-state concentration of *qrr* and HapR in each strain and normalized them by their wild-type values. The data (left), results from our model (middle), and corresponding error (right) are shown in figure 11. Our results are in good qualitative and quantitative agreement with the data.

3.2.3. Dosage compensation and Qrr feedback. To show that regulation in the sRNA circuit is responsible for dosage compensation, Svenningsen *et al* measured luminescence in a wild-type, $\Delta hapR$, and in a *luxOAUCC* strain (a strain lacking the LuxO-Qrr feedback) with and then without all Qrr. Assuming the stability of each *qrr-lux* construct is the same and that fluorescence is proportional to the concentration of *qrr*, we normalized their data by the fluorescence from the *qrr1-lux* construct in the $\Delta hapR\Delta qrr1{-}4$ strain. The data, in figure 12, show that removing one or more *qrr* increases expression of the remaining *qrr*.

To model this experiment we created a parameterization of each strain. For the $\Delta hapR$ strain, we set $E_{r_n} = \widehat{K}_{L_n} = 0$ for all n and, for the *luxOAUCC* strain, we set $E_{o_n} = V_{or} = 0$ for all n. To remove Qrr from these strains, we set $\widehat{K}_{P_n} = 0$ for all n. The model of each *qrr-lux* construct is identical to our model of the Qrr promoter in (24), i.e.

$$C_n(r, o) = \frac{\widehat{K}_{P_n}\Gamma o}{1 + \widehat{K}_{P_n}\Gamma o}\frac{1 + V_{q_n}(\widehat{K}_{L_n} r)^2}{1 + (\widehat{K}_{L_n} r)^2}. \qquad (27)$$

We computed the steady state concentration of r and o in each strain with and then without Qrr then evaluated (27) at each steady state. We then normalized the luminescence from each promoter by its corresponding luminescence from the wild-type promoter. Our results, figure 12 (middle), show that the model agrees well with the data both qualitatively and quantitatively.

As an extension to the above experiment, Svenningsen *et al* created a strain without the LuxO-Qrr feedback and examined the fold change in *qrr-lux* luminescence in a strain with versus without Qrr. Their results, in figure 13 (left), show that *qrr3* is most sensitive to changes in *qrr* whereas there is a more modest change in the remaining *qrr*.

To model this experiment, we took the wild-type strain parameterization and set $E_{o_n} = 0$ for all n to remove the LuxO-Qrr feedback. We then found the steady-state concentrations of HapR and LuxO in a strain with and then without *qrr*. We used these steady-states to evaluate (27) to, again, determine the luminescence from each *qrr-lux* construct. Lastly, we normalized the luminescence of each $qrr{-}lux$ in the $\Delta qrr1{-}4$ strain by the luminescence in the strain with all *qrr*. Figure 13 shows that our model (middle) agrees well with the data (left).

3.3. Parameter uncertainty

To get an idea of what parameters are reliably estimated from the experiments by our model, we studied the linearization of $\boldsymbol{F}(\boldsymbol{p})$ at the parameterization determined in the previous section. If $\delta\boldsymbol{p}$ is small, then $\boldsymbol{F}(\boldsymbol{p} + \delta\boldsymbol{p}) = \boldsymbol{F}(\boldsymbol{p}) + D\boldsymbol{F}(\boldsymbol{p})\delta\boldsymbol{p} + O(||\delta\boldsymbol{p}||^2)$. Therefore, if each element in the column of $D\boldsymbol{F}(\boldsymbol{p})$ corresponding to parameter p_j is small (i.e. $\left|\frac{\partial F_i(\boldsymbol{p})}{\partial p_j}\right| \ll 1$ for all i), then the data is not very sensitive to p_j and we cannot expect to estimate the parameter reliably using the data.

We found that $\boldsymbol{F}(\boldsymbol{p})$ and $D\boldsymbol{F}(\boldsymbol{p})$ are accurate up to an order of 10^{-10}. Evaluating $\boldsymbol{F}(\boldsymbol{p})$ and $D\boldsymbol{F}(\boldsymbol{p})$ involves solving for the

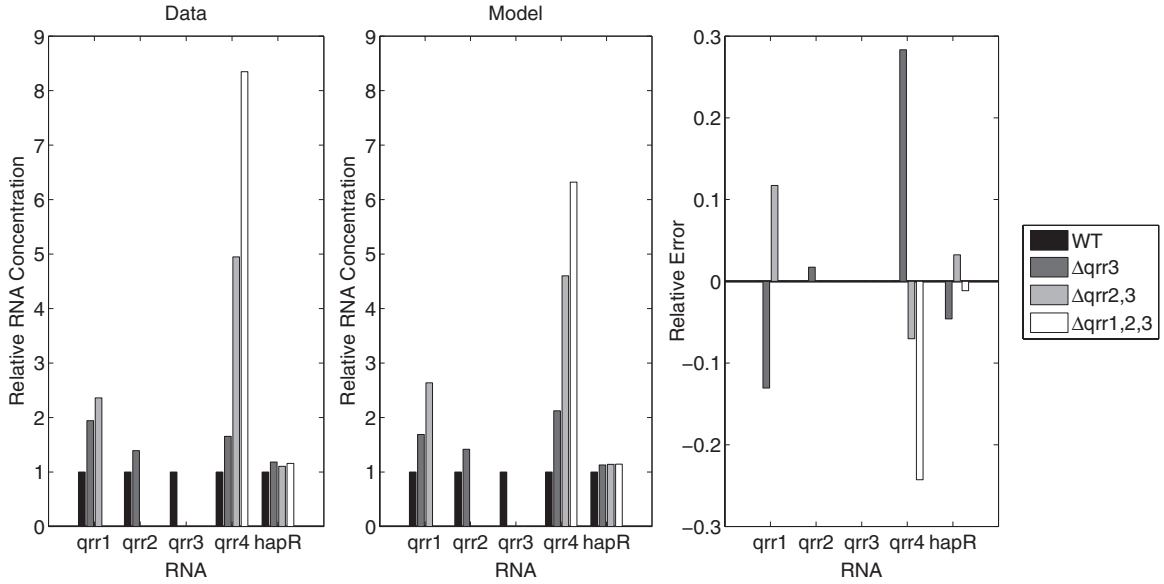

Figure 11. Comparison of the dosage compensation response for each Qrr between the data [29] (left) and our results (middle). Expression of each *qrr* increases relative to their wild-type concentrations at LCD when Qrr are sequentially removed. The error (right) shows that the model agrees well with the data overall.

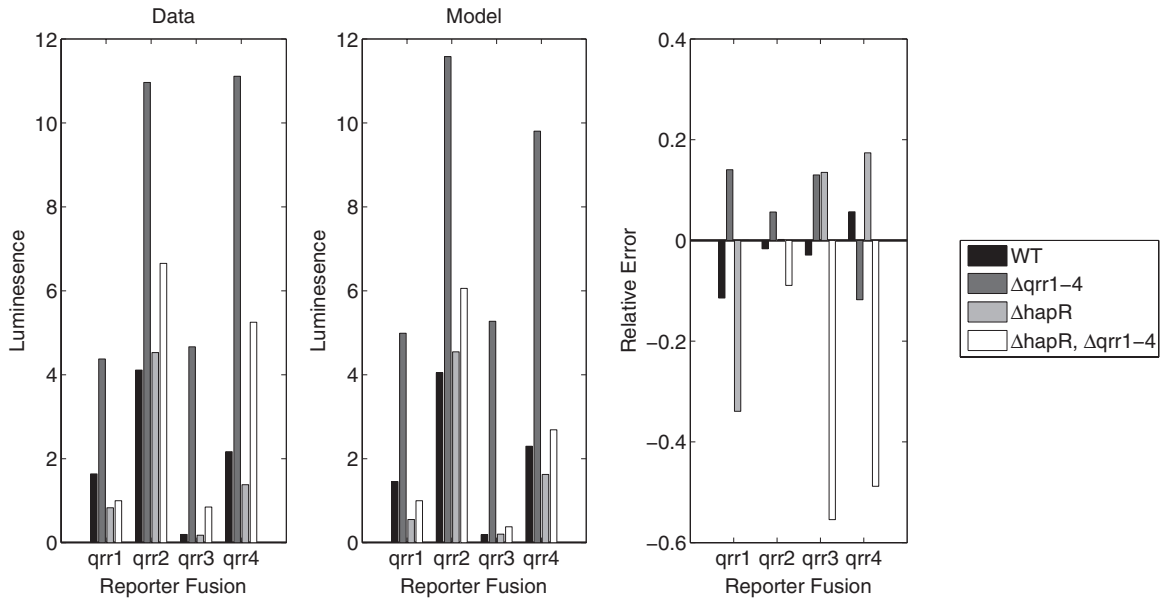

Figure 12. Comparison between the data [29] (left) and our results (middle) showing the fold change in *qrr-lux* luminescence in strains with and/or without Qrr and/or HapR. Luminescence from each construct is presented relative to *qrr1-lux* luminescence in the Δ*hapR* strain. The error (right) shows that our results agree well with the data.

steady-states with a nonlinear solver that starts with a random initial guess. Hence even with the same parameterization $\boldsymbol{p}$ the values of the forward map and its Jacobian may be slightly different from one simulation to another. We evaluated $\boldsymbol{F}(\boldsymbol{p})$ and $D\boldsymbol{F}(\boldsymbol{p})$ multiple times using the same parameterization and found that they differ up to 10^{-10} element-wise. Therefore, we assume that the jth parameter is a stationary solution of $\boldsymbol{F}(\boldsymbol{p}) = \boldsymbol{d}$ if $\left|\frac{\partial F_i(\boldsymbol{p})}{\partial p_j}\right| \leqslant 10^{-9}$ for all i. We examined each column of the Jacobian and found that there was at least one element in each column greater than 10^{-9}. This suggests that we could identify all of the parameters for each species using the data. Our results are summarized in figure 14 where we show the column norm of the Jacobian for the corresponding parameter.

This result also shows that *V. cholerae* parameters are more easily distinguished than the *V. harveyi* parameters and that *V. harveyi* E_{r_1} is the hardest parameter to distinguish in the data. This may explain why E_{r_1} is around 10^2 fold larger than the other E_{r_n} in *V. harveyi*. This is somewhat expected given that the bulk of the *V. harveyi* data were very similar (i.e. showing LuxR-mCherry fluorescence as a function of autoinducer) rather than the output from a variety of mutant strains.

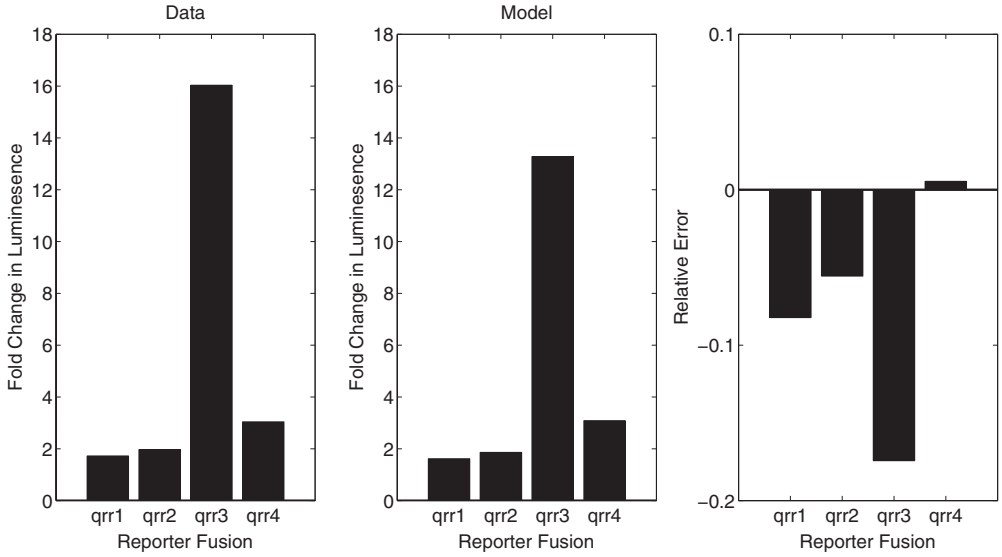

Figure 13. Comparison between the data [29] (left) and our results (middle) showing the fold change in *qrr-lux* luminescence when Qrr are removed in a strain without the LuxO-Qrr feedback. The error (right) shows that the model agrees well with the data.

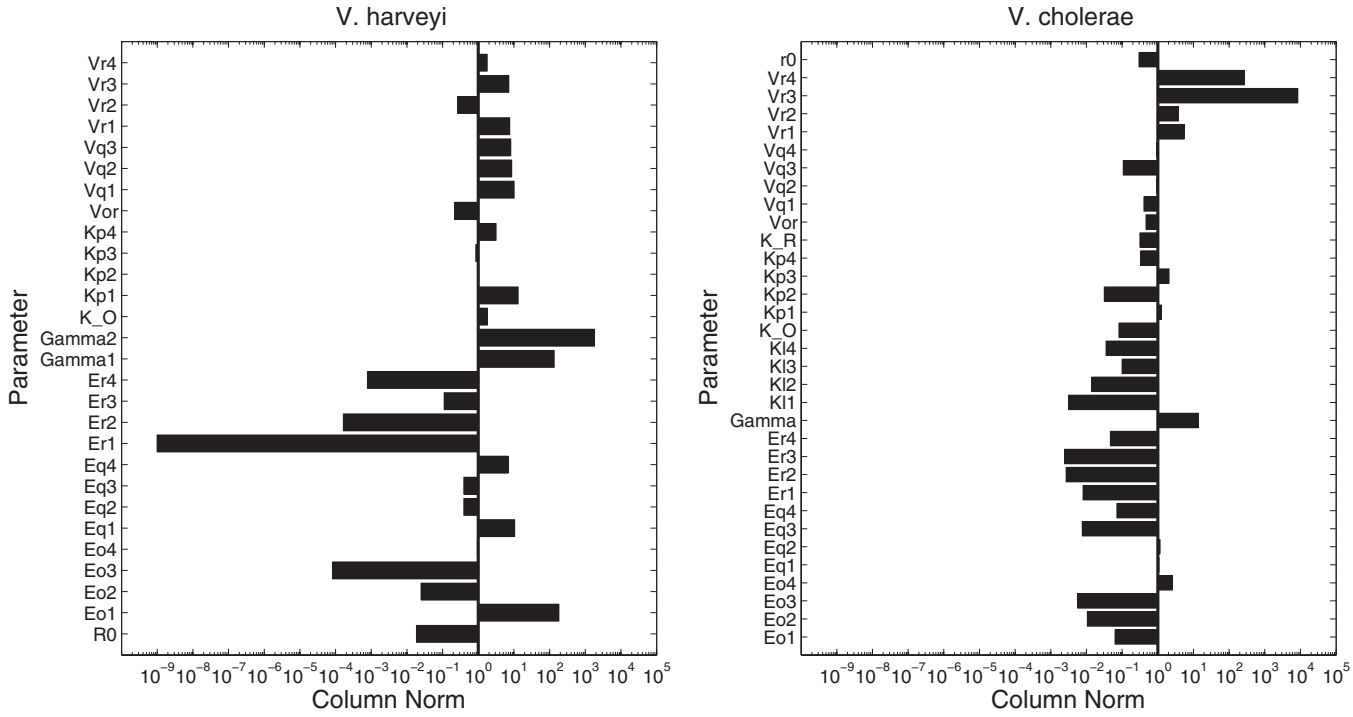

Figure 14. Comparison of the column norms of $DF(\boldsymbol{p})$ for each parameter in *V. harveyi* and *V. cholerae*. The parameter corresponding to the column of the Jacobian is shown on the vertical axis, while the norm of the column is on the horizontal axis.

To understand the parameter identification further, we computed the singular value decomposition of the Jacobian matrix to see what linear combination of parameters was associated with the smallest singular values and, hence, weak search directions. Overall, we found that the parameters associated with the smallest column norm of the Jacobian are also the main components of the right-singular vectors associated with the smallest singular values (see table 2). These results again show that $E_{r_1}, E_{r_2}, E_{r_4}$, and E_{o_3} are difficult to identify in the *V. harveyi* data whereas E_{o_1}, E_{o_3}, E_{o_4}, E_{q_3}, E_{q_4}, E_{r_2}, E_{r_3}, Γ, K_{p_3}, and V_{q_2} are difficult to identify for *V. cholerae*. These results show that both the *V. harveyi* and *V. cholerae* parameterizations will benefit from new experiments that target these specific parameters.

Up to now we have only used the Jacobian of the forward map. To account for the nonlinearity of the problem we also generated 250 different realizations of the data by randomly perturbing the data by at most 10% with a uniformly distributed random number. We then parameterized the model to each realization of the data by solving the problem in (26) and

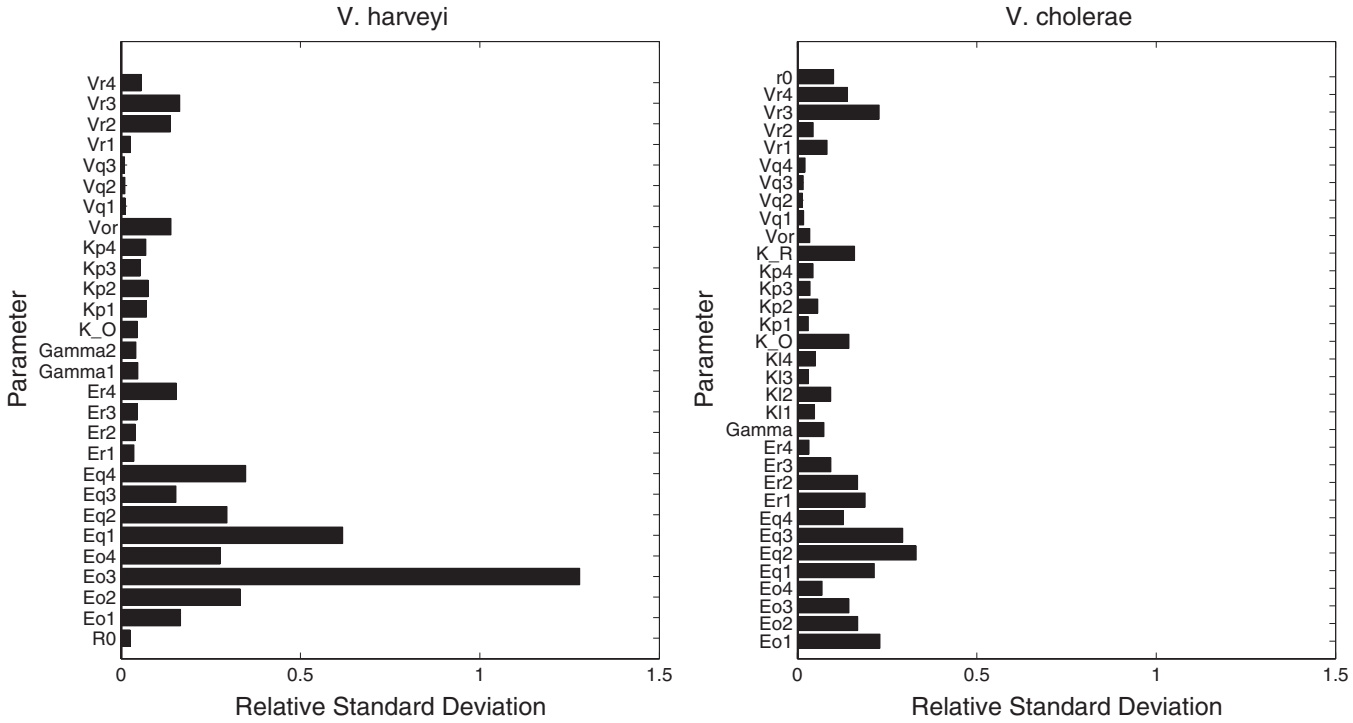

Figure 15. The standard deviation of each parameter in *V. harveyi* (left) and *V. cholerae* (right) relative to its corresponding value in table 1. We generated 250 new synthetic data by randomly perturbing the empirical data by at most 10%.

Table 2. Coefficients of the right-singular vectors associated with the small singular values of the Jacobian for *V. harveyi* and *V. cholerae* that are 10^{-7} smaller than the largest singular value. We ignored coefficients smaller than 0.1 in absolute value.

V. harveyi

	σ_{n-3}	σ_{n-2}	σ_{n-1}	σ_n
E_{o_3}	1.0	–	–	–
E_{r_1}	–	–	–	−1.0
E_{r_2}	–	−0.1	1.0	–
E_{r_4}	–	−1.0	−0.1	–

V. cholerae

	σ_{n-7}	σ_{n-6}	σ_{n-5}	σ_{n-4}	σ_{n-3}	σ_{n-2}	σ_{n-1}	σ_n
E_{o_1}	–	−0.2	−0.5	−0.9	–	–	–	–
E_{o_3}	−0.1	1.0	−0.3	–	–	–	–	–
E_{o_4}	–	–	–	–	1.0	–	–	–
E_{q_3}	–	–	0.1	–	–	–	–	–
E_{q_4}	–	0.2	0.8	−0.5	–	–	–	–
E_{r_2}	–	–	–	–	–	–	–	−1.0
E_{r_3}	–	–	–	–	–	−0.1	1.0	–
Γ	–	–	–	–	–	−1.0	−0.1	–
K_{p_3}	−1.0	−0.1	–	–	–	–	–	–
V_{q_2}	–	–	−0.1	–	–	–	–	–

using the parameterization of each species in table 1 as the initial estimate. We divided the standard deviation of each parameter by its corresponding value in table 1 and present our results in figure 15. We see that most of the parameters change on an order similar to the order of the error in the data. Therefore, with the exception of a few parameters, the *parameter estimation* for both *V. harveyi* and *V. cholerae* is robust, in the sense that errors in the data give similar parameters. To quantify the uncertainty in the parameters given the measured data more rigorously we would need to do a Bayesian estimation (Monte Carlo analysis). Because the cost of evaluating the forward problem and the necessary number of realizations involved in a Monte Carlo analysis was prohibitive, such analysis was not carried out here.

Therefore, some parameters in our model cannot be reliably estimated from the experimental data that we consider. However, new experiments could be designed to specifically target these unresolved parameters and complete the model.

3.4. Species comparisons and qualitative predictions

Although the sRNA circuits in *V. harveyi* and *V. cholerae* are topologically equivalent, the parameterization for each species is different. Here we use our model to consider a series of experiments designed to identify qualitative differences in the responses of *V. harveyi* and *V. cholerae* and to understand the mechanisms responsible for these differences. Our results show that abundance of Hfq-Qrr and changes to LuxO via the LuxO-Qrr feedback drive changes in *V. cholerae* Qrr concentration at LCD. Conversely, Hfq-Qrr is less abundant and Qrr less sensitive to changes in target mRNA in *V. harveyi*. We, therefore, argue and show that dosage compensation is stronger in *V. cholerae* than in *V. harveyi* and that HapR is less sensitive than LuxR to changes in Qrr.

In what follows, we compare the fold change of *qrr4* concentration with the fold change in *qrr4* promoter activity between various strains. We measure *qrr4* concentration by modeling a real-time PCR analysis experiment and measure *qrr4* promoter activity by modeling the luminescence from a *qrr4-lux* construct. If the fold change in *qrr4* concentration

Table 3. Activation at the *qrr* promoter and Hfq determines the fold change in *qrr*4 expression. Differences between the fold change of *qrr4* concentration compared to the fold change in *qrr4-lux* luminescence shows the degree to which a change in *qrr4* concentration is driven by a change in *qrr*4 activation versus Hfq.

		qrr4 concentration		*qrr4-lux* luminescence	
Expression in...	Relative to...	*V. harveyi*	*V. cholerae*	*V. harveyi*	*V. cholerae*
ΔQrr feedback	ΔQrr feedback −LuxR/HapR	0.88	0.75	1.00	1.00
ΔLuxO-Qrr feedback	ΔQrr feedback	1.61	1.53	1.59	1.19
WT	ΔLuxO-Qrr feedback	0.86	0.042	0.89	0.71

is similar to the fold change in *qrr4-lux* luminescence, then the change in *qrr4* concentration is driven by a change in its expression rather than a change in its degradation via Hfq. Therefore, by comparing the fold change in *qrr4* concentration with the fold change in *qrr4* promoter activity, we can understand the degree to which changes in Hfq affect *qrr4* levels.

We begin by modifying the wild-type parameterization to create parameterizations for three different mutant strains: ΔLuxO-Qrr feedback ($E_{o_n} = 0$), ΔQrr feedback ($E_{o_n} = \widehat{K}_{L_n} = 0$), and ΔQrr feedback−LuxR/HapR ($E_{o_n} = E_{r_n} = \widehat{K}_{L_n} = 0$). For each strain including the wild-type strain, we compute the steady-state concentration of *qrr4*, *luxR/hapR*, and *luxO* at LCD ($\Gamma = \Gamma_{\mathrm{LCD}}$). We use the steady-state concentration of *luxR/hapR* and *luxO* in (27) to measure the *qrr4-lux* luminescence for that particular strain. The *qrr4-lux* construct has the same mutations as the mutant strain (i.e. the model of the *qrr4-lux* construct for the ΔQrr feedback strain has $\widehat{K}_{L_n} = 0$). Lastly, we compare the fold change in *qrr4* concentration and in *qrr4-lux* luminescence between the strains indicated in table 3. The results identify how Hfq and Qrr feedback regulate the concentration of *qrr4* in *V. harveyi* and *V. cholerae* at LCD.

The first row of table 3 shows that addition of LuxR/HapR decreases *qrr4* in *V. cholerae* more than in *V. harveyi* because Hfq-Qrr is less abundant in *V. cholerae* than in *V. harveyi* in the absence of Qrr feedback. Note that *qrr4-lux* luminescence is constant because Qrr feedback is absent from both strains, so the change in *qrr4* concentration is driven by the change in Hfq-Qrr. In a ΔQrr feedback −LuxR/HapR strain, there is no target mRNA for Qrr to repress, so all available Hfq is bound by Qrr (i.e. $\sum_{n=1}^{4} H_n = 1$). On reintroducing LuxR/HapR, Qrr unbinds Hfq to repress LuxR/HapR. This diminishes the concentration of Hfq-Qrr and *qrr4* because more Hfq is available for it to bind. Therefore, Hfq-Qrr is less abundant in *V. cholerae* than in *V. harveyi* in the absence of Qrr feedback because *qrr4* decreases more in *V. cholerae* than in *V. harveyi*.

The second row of table 3 shows that *qrr4* increases when the LuxR/HapR-Qrr feedback is reintroduced because LuxR/HapR enhances *qrr4* expression. This also shows that the concentration of Hfq-Qrr in the ΔLuxO-Qrr feedback strain is similar to that in a ΔQrr feedback strain because the change in *qrr4-lux* luminescence is similar to the change in *qrr4* concentration. Therefore, although *qrr4* increases more in *V. harveyi* than in *V. cholerae*, *V. cholerae qrr4* remain less abundant than *V. harveyi qrr4*.

The last row of table 3 shows that *qrr4* decreases more in *V. cholerae* than in *V. harveyi* when the LuxO-Qrr feedback is reintroduced because *V. cholerae qrr*4 is more sensitive to changes in LuxO. The LuxO-Qrr feedback represses LuxO, so we expect that *qrr4* concentration will decrease as it does for both species. We see that the change in *qrr*4−*lux* luminescence is comparable between the two species, so the changes in *qrr*4 concentration arise from differences in the sensitivity of their respective *qrr*4 promoter to changes in LuxO. Given the significantly greater decrease in *V. cholerae qrr*4 relative to the *V. harveyi qrr*4 concentration, we, therefore, conclude that *V. cholerae qrr*4 is more sensitive to changes in LuxO than *V. harveyi qrr*4. When we compare the fold changes in *qrr*4 concentration between the second and third rows of table 3, we also conclude that *V. harveyi* and *V. cholerae* are approximately equally sensitive to changes in LuxR/HapR, but that *V. cholerae qrr*4 is significantly more sensitive than *V. harveyi qrr*4 to changes in LuxO. These results were similar across all Qrr in *V. harveyi* and *V. cholerae*.

Table 4. Fold change in *qrr4*, LuxR/HapR, and LuxO in a $\Delta qrr1-3$ strain relative to a wild-type strain at LCD for *V. harveyi* and *V. cholerae*.

	Fold change in...		
Species	*qrr*4	*luxR*/*hapR*	*luxO*
V. harveyi	1.71	5.25	2.55
V. cholerae	6.32	1.14	3.16

The above results suggest that dosage compensation is driven by changes in LuxO only in *V. cholerae* and by changes in LuxR and/or LuxO in *V. harveyi*. To test this, we measured the fold change in *qrr*4, *luxR*/*hapR*, and *luxO* in *V. harveyi* and *V. cholerae* in a wild-type strain relative to a $\Delta qrr1-3$ strain. As expected, *qrr*4 concentration increases in the $\Delta qrr1-3$ strain for both species (see table 4). We also see that *luxR* and *luxO* increased significantly, whereas only *hapR* increased marginally. These results reflect the different sensitivities of the Qrr promoter to target mRNA. Dosage compensation of Qrr (i.e. the fold change in *qrr*4) arises when the expression of Qrr is sensitive to changes in target mRNA and when target mRNA is sensitive to changes in Qrr via Hfq. Given that *V. cholerae qrr*4 is significantly more sensitive to changes in LuxO than HapR, dosage compensation in *V. cholerae* is primarily driven by changes in LuxO. Similarly, *V. harveyi* Qrr are sensitive to changes in both LuxR and LuxO, so dosage compensation in *V. harveyi* is driven by changes in LuxR and LuxO.

4. Conclusion and outlook

Quorum sensing systems are gene regulatory mechanisms that enable bacteria to regulate their gene expression based on the local cell-population density. *V. harveyi* and *V. cholerae* are virulent marine bacteria that use a quorum sensing system to regulate expression of their respective virulence factors and, for *V. harveyi*, bioluminescence. Their quorum sensing systems are comprised of a phosphorelay cascade that integrates cell-population density information and an sRNA circuit that regulates expression of quorum sensing target genes [7]. Studies show that, even though their quorum sensing systems are topologically equivalent and homologous, HapR is more robust than LuxR to changes in Qrr [16, 17]. In this work, we formulate and parameterize a novel mathematical model of the *V. harveyi* and *V. cholerae* sRNA circuit to explain these kinetic differences.

We showed that our model and parameters are representative of the *V. harveyi* and *V. cholerae* sRNA circuit. We derived our model using known reaction kinetics and then fit the model to a variety of empirical data by solving a nonlinear least-squares problem. We found that the model agrees well with all of the available data and the data is sufficient to identify most of the parameters. The overall good correspondence between the model and data along with the general reliability of our parameterization implies that the current understanding of the biology is sufficient to explain a wide variety of behaviors. In particular, the details of how HapR enhances Qrr expression and the role of a third phosphorelay cascade in *V. cholerae* are unnecessary to understand its quorum sensing response.

We have shown that our model can be used to identify novel kinetic differences and their underlying mechanisms, whereas the topological and genetic similarities make this difficult to do so experimentally. We considered a set of experiments that compare the change in Qrr concentration with the change in the luminescence from a *qrr-lux* construct. Comparing these measures allows us to determine the degree to which a change in Qrr levels is driven by a change in Hfq rather than a change in the Qrr promoter activity.

Svenningsen *et al* showed that Qrr feedback causes dosage compensation of Qrr and, therefore, argued that Qrr feedback is the mechanism underlying the robust repression of LuxR/HapR [29]. In view of our results, we argue that, if dosage compensation is the mechanism underlying redundancy and repression of LuxR/HapR is robust, then dosage compensation is driven by changes in LuxO via the LuxO-Qrr feedback. Dosage compensation requires that Qrr expression is sensitive to changes in target mRNA and that target mRNA expression is sensitive to changes in Qrr via Hfq-Qrr. If repression of LuxR/HapR is robust, then LuxR/HapR remains relatively constant to changes in Qrr, so LuxO is the only target mRNA remaining to change Qrr expression and, hence, drive dosage compensation. Therefore, if repression of LuxR/HapR is robust to changes in Qrr, then dosage compensation of Qrr is necessarily driven by changes in LuxO.

Our model can be used to design novel experiments to improve our parameterizations and to validate the model with independent data (for similar discussions see [37–40]). Our parameterizations will be improved by designing experiments that specifically target the parameters with the greatest uncertainty because, as we have shown, there is little benefit parameterizing the model to new realizations of the same data. To this end, we have provided the tools and framework to identify the least certain parameters and how new experiments may yield more information about those parameters. In particular, we have shown how to model a variety of different experiments with our model, which can be extended to model new experiments. The columns of the Jacobian of $\boldsymbol{F}(\boldsymbol{p})$ and its SVD can then identify the parameters that will remain uncertain after the experiments. Lastly, the marginal benefit associated with each realization of the data can be assessed by computing the relative standard deviation of each parameter in the process described previously.

Our work supports the hypothesis that the *V. harveyi* and *V. cholerae* quorum sensing circuits are topologically equivalent, yet tuned differently to elicit different responses [7]. With the aid of our model, we identified how *V. harveyi* and *V. cholerae* are tuned differently. To our knowledge, this is the first detailed model of the *V. harveyi* and *V. cholerae* sRNA circuits with physiologically-based estimates of the parameters. As such, our parameters can be used in similar models and our model can help design more quantitative experiments in the future.

5. Abbreviations list

sRNA, small RNA; Qrr, quorum regulated RNA.

Acknowledgments

The authors thank Dr Bonnie Bassler, Dr Kim Tu, and Dr Sine Svenningsen for helpful discussions and for sharing their raw data. We also thank Dr Kelly M Winterberg and Dr Elizabeth D Copene for their helpful comments preparing this manuscript. The work of Dr James P Keener was partially supported by the National Science Foundation grant DMS-1122297 and the work of Dr Fernando Guevara Vasquez was partially supported by the National Science Foundation grant DMS-0934664.

References

[1] Dockery J and Keener J 2001 A mathematical model for quorum sensing in *Pseudomonas aeruginosa* *Bull. Math. Biol.* **63** 95–116

[2] Ruby E G and Nealson K H 1976 Symbiotic association of *Photobacterium fischeri* with the marine luminous fish *Monocentris japonica*; a model of symbiosis based on bacterial studies *Biol. Bull.* **151** 574–86

[3] Schuster M, Phoebe Lostroh C, Ogi T and Greenberg E P 2003 Identification, timing, and signal specificity of *Pseudomonas aeruginosa* quorum-controlled genes: a transcriptome analysis *J. Bacteriol.* **185** 2066–79

[4] Keller L and Surette M G 2006 Communication in bacteria: an ecological and evolutionary perspective *Nature Rev. Microbiol.* **4** 249–58

[5] Whitehead N A, Barnard A M, Slater H, Simpson N J and Salmond G P 2001 Quorum-sensing in gram-negative bacteria *FEMS Microbiol. Rev.* **25** 365–404

[6] Fuqua C, Winans S C and Peter Greenberg E 1996 Census and consensus in bacterial ecosystems: the LuxR-LuxI family of quorum-sensing transcriptional regulators *Annu. Rev. Microbiol.* **50** 727–51

[7] Ng W-L and Bassler B L 2009 Bacterial quorum-sensing network architectures *Annu. Rev. Genet.* **43** 197–222

[8] Wilson T and Hastings J W 1998 Bioluminescence *Annu. Rev. Cell Dev. Biol.* **14** 197–230

[9] Waters C M and Bassler B L 2005 Quorum sensing: cell-to-cell communication in bacteria *Annu. Rev. Cell Dev. Biol.* **21** 319–46

[10] Henke J M and Bassler B L 2004 Bacterial social engagements *Trends Cell Biol.* **14** 648–56

[11] Rutherford S T and Bassler B L 2012 Bacterial quorum sensing: its role in virulence and possibilities for its control *Cold Spring Harb. Perspect. Med.* **2** doi:10.1101/cshperspect.a012427

[12] Ng W-L, Perez L, Cong J, Semmelhack M F and Bassler B L 2012 Broad spectrum pro-quorum-sensing molecules as inhibitors of virulence in vibrios *PLoS Pathogens* **8** e1002767

[13] Ng W-L, Perez L J, Wei Y, Kraml C, Semmelhack M F and Bassler B L 2011 Signal production and detection specificity in vibrio CqsA/CqsS quorum-sensing systems *Mol. Microbiol.* **79** 1407–17

[14] Wei Y, Perez L J, Ng W-L, Semmelhack M F and Bassler B L 2011 Mechanism of *Vibrio cholerae* autoinducer-1 biosynthesis *ACS Chem. Biol.* **6** 356–65

[15] Henke J M and Bassler B L 2004 Three parallel quorum-sensing systems regulate gene expression in *Vibrio harveyi J. Bacteriol.* **186** 6902–14

[16] Lenz D H, Mok K C, Lilley B N, Kulkarni R V, Wingreen N S and Bassler B L 2004 The small RNA chaperone hfq and multiple small RNAs control quorum sensing in *Vibrio harveyi* and *Vibrio cholerae Cell* **118** 69–82

[17] Tu K C and Bassler B L 2007 Multiple small RNAs act additively to integrate sensory information and control quorum sensing in *Vibrio harveyi Genes Dev.* **21** 221–33

[18] Bejerano-Sagie M and Bivar Xavier K 2007 The role of small RNAs in quorum sensing *Curr. Opin. Microbiol.* **10** 189–98

[19] Tu K C, Long T, Svenningsen S L, Wingreen N S and Bassler B L 2010 Negative feedback loops involving small regulatory RNAs precisely control the *Vibrio harveyi* quorum-sensing response *Mol. Cell* **37** 567–79

[20] Stewart P S 2003 Diffusion in biofilms *J. Bacteriol.* **185** 1485–91

[21] Neiditch M B, Federle M J, Miller S T, Bassler B L and Hughson F M 2005 Regulation of LuxPQ receptor activity by the quorum-sensing signal autoinducer-2 *Mol. Cell* **18** 507–18

[22] Neiditch M B, Federle M J, Pompeani A J, Kelly R C, Swem D L, Jeffrey P D, Bassler B L and Hughson F M 2006 Ligand-induced asymmetry in histidine sensor kinase complex regulates quorum sensing *Cell* **126** 1095–108

[23] Wei Y, Ng W-L, Cong J and Bassler B L 2012 Ligand and antagonist driven regulation of the *Vibrio cholerae* quorum-sensing receptor CqsS *Mol. Microbiol.* **83** 1095–108

[24] Nadell C D and Bassler B L 2011 A fitness trade-off between local competition and dispersal in *Vibrio cholerae* biofilms *Proc. Natl Acad. Sci. USA* **108** 14181–5

[25] van Kessel J C, Rutherford S T, Shao Y, Utria A F and Bassler B L 2013 Individual and combined roles of the master regulators AphA and LuxR in control of the *Vibrio harveyi*quorum-sensing regulon *J. Bacteriol.* **195** 436–43

[26] Shao Y and Bassler B L 2012 Quorum-sensing non-coding small RNAs use unique pairing regions to differentially control mRNA targets *Mol. Microbiol.* **83** 599–611

[27] Tu K C, Waters C M, Svenningsen S L and Bassler B L 2008 A small-RNA-mediated negative feedback loop controls quorum-sensing dynamics in *Vibrio harveyi Mol. Microbiol.* **70** 896–907

[28] Long T, Tu K C, Wang Y, Mehta P, Ong N P, Bassler B L and Wingreen N S 2009 Quantifying the integration of quorum-sensing signals with single-cell resolution *PLoS Biol.* **7** e1000068

[29] Svenningsen S L, Tu K C and Bassler B L 2009 Gene dosage compensation calibrates four regulatory RNAs to control *Vibrio cholerae* quorum sensing *EMBO J.* **28** 429–39

[30] Swem L R, Swem D L, Wingreen N S and Bassler B L 2008 Deducing receptor signaling parameters from in vivo analysis: LuxN/AI-1 quorum sensing in *Vibrio harveyi Cell* **134** 461–73

[31] Patrick Bardill J, Zhao X and Hammer B K 2011 The vibrio cholerae quorum sensing response is mediated by hfq-dependent sRNA/mRNA base pairing interactions *Mol. Microbiol.* **80** 1381–94

[32] Chatterjee J, Miyamoto C M and Meighen E A 1996 Autoregulation of *luxR* : the *Vibrioharveyilux* -operon activator functions as a repressor *Mol. Microbiol.* **20** 415–25

[33] Lin W, Kovacikova G and Skorupski K 2005 Requirements for vibrio cholerae HapR binding and transcriptional repression at the hapR promoter are distinct from those at the aphA promoter *J. Bacteriol.* **187** 3013–9

[34] Svenningsen S L, Waters C M and Bassler B L 2008 A negative feedback loop involving small RNAs accelerates *Vibrio choleraes* transition out of quorum-sensing mode *Genes Dev.* **22** 226–38

[35] Geissmann T A and Touati D 2004 Hfq, a new chaperoning role: binding to messenger RNA determines access for small RNA regulator *EMBO J.* **23** 396–405

[36] Brennan R G and Link T M 2007 Hfq structure, function and ligand binding *Curr. Opin. Microbiol.* **10** 125–33

[37] Casey F P, Baird D, Feng Q, Gutenkunst R N, Waterfall J J, Myers C R, Brown K S, Cerione R A and Sethna J P 2007 Optimal experimental design in an epidermal growth factor receptor signalling and down-regulation model *IET Syst. Biol.* **1** 190–202

[38] Apgar J F, Witmer D K, White F M and Tidor B 2010 Sloppy models, parameter uncertainty, and the role of experimental design *Mol. Biol. Syst.* **6** 1890–900

[39] Bandara S, Schloder J P, Eils R, Bock H G and Meyer T 2009 Optimal experimental design for parameter estimation of a cell signaling model *PLoS Comput. Biol.* **5** e1000558

[40] Versyck K J, Bernaerts K, Geeraerd A H and Van Impe J F 1999 Introducing optimal experimental design in predictive modeling: a motivating example *Int. J. Food Microbiol.* **51** 39–51